Chemical Physics Letters 826 (2023) 140637

Contents lists available at ScienceDirect

Chemical Physics Letters

journal homepage: www.elsevier.com/locate/cplett

Research paper

Dual-frequency switchable bandpass filter in the terahertz range based on enhanced trapped-mode resonances

Yi Zhang [a,1], Dongxun Yang [a,1], Dan Zhao [b], Danni Hao [a], Pinggen Zou [a], Yanmei Ren [a], Rui Li [a], Xiaodong Zhu [a], Fei Fan [b], Shengjiang Chang [b], Ramiro Moro [a], Lei Ma [a,*]

[a] Tianjin International Center for Nanoparticles and Nanosystems, Tianjin University, Tianjin 300072, China
[b] Institute of Modern Optics, Nankai University, Tianjin Key Laboratory of Micro-scale Optical Information Science and Technology, Tianjin 300350, China

ARTICLE INFO

Keywords:
Metamaterial
Optical devices
Modulator
Terahertz

ABSTRACT

We propose a high-quality and mechanically tunable dual-band narrow bandpass filter working in the THz range. Its high transmittance and modulation depth are verified both by simulations and experiments. The proposed design consists of two metasurfaces with concentric fabricated *meta*-atoms back-to-back on the two sides of a thin polyimide layer. When the polarization of the incident THz waves changes from y to × direction, the modulation depth of transmittance monotonically changes from 95.46% to a few percent at the resonance frequencies of 0.481 THz and inversely varies from a few percent to 97.62% at the resonance frequency of 0.931 THz. The analysis of in-plane and inter-planar distributions of induced surface current reveals that the narrow bandpass response is attributed to the excitation of "trapped mode". The induced antiphase current excitation between the two metasurfaces not only lower the dipole moment but also weakly couple to external electromagnetic fields, consequently, leading to the high transmittance and narrow bandwidth. These features of such a simple device potentially can contribute to the design of much more advanced THz modulators and other THz applications in the future.

1. Introduction

Much efforts have been devoted to develop terahertz (THz) devices due to their vast applications in bio-sensing [1,2], security [3,4], molecular spectroscopy [5], and ultra-fast communications [6]. Despite their rapid progress, it still confronts dillima between the absences of THz devices such as wave generators [7], modulators [8], and detectors [9] and even faster grown needs in science and industry. One main barricade is that compared to microwave and photonics technologies, there are short of materials with strong THz-responding in nature [10]. While, recently developed microfabrication based metamaterials with artificial subwavelength unit provide one of most promising solution [11,12]. By rational structure design, they can have extraordinary electromagnetic (EM) properties right meet the THz-regime devices needs, such as filters [13,14], modulators [15,16], switches [17], and absorbers [18,19].

Narrow bandpass filters are of the most essential THz devices, which are characterized by the high Q-value and transmittance [20]. However, conventional planar metamaterials commonly have rather low resonance quality factors and fixed filtering band, which largely limits the scope of their applications. Moreover, recent reports have proposed several tunable THz filters through external modulations, such as Fermi level tunning through variation of gating voltage [21–23], dramatic conductivity adjusting through insulator–metal transition by controlling temperature [24,25], *meta*-atom geometry tunning and lattice constant adjustment through mechanical deformation by applying external force field [26,27], electromagnetic excitation through optical pumping [28,29] and impinging wave modulation by rotation of polarization-sensitive structures has also been reported [30,31].

Although, much effort has been devoted, the challenge still remains. It pressingly needs to develop simply fabricated, easy-modulating, and well-performing bandpass filters to break the limits. In principle, the polarization-sensitive structures with mechanical tunability could realize THz modulation with rather reliable performance. However, few results are reported so far [32].

In this paper, we propose a switchable mechanical dual-frequency

* Corresponding author.
E-mail address: lei.ma@tju.edu.cn (L. Ma).
[1] These two authors contribute equally.

https://doi.org/10.1016/j.cplett.2023.140637
Received 5 December 2022; Received in revised form 26 April 2023; Accepted 1 June 2023
Available online 12 June 2023
0009-2614/

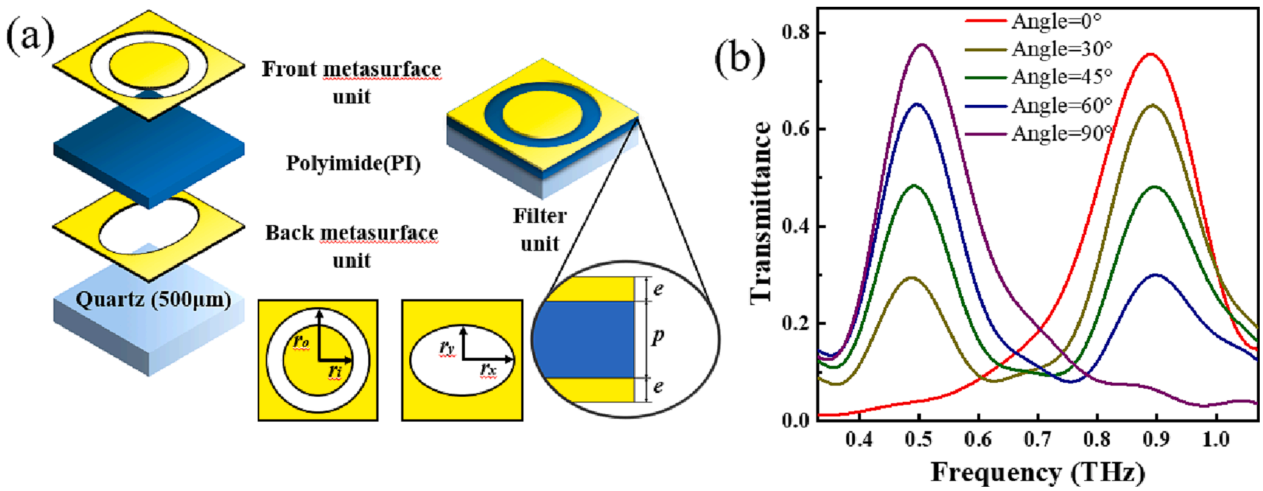

Fig. 1. (a) Schematic configuration of the *meta*-atoms of the bandpass filter. (b) The simulated transmittance spectra of electromagnetic wave with different polarization angles.

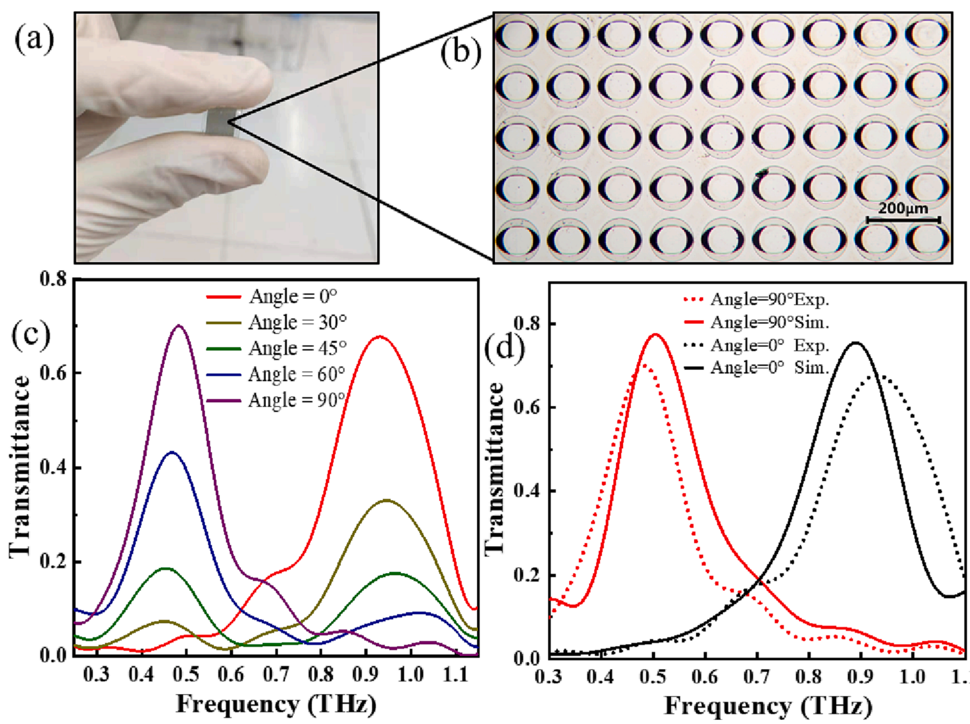

Fig. 2. (a) The appearance of the bandpass filter device. (b) The top view graph of the device by the optical microscope (VIYEE Optical WY-2000 M). (c) Experimentally measured transmittance spectrum in the frequency domain with rotation angles of 0°, 30°, 45°, 60°, and 90°. (d) Experimentally measured transmittance spectra of the device corresponding to two typical rotation angles (0° and 90°).

narrow bandpass filter in the THz range. Structually it is easily to be fabricated which is composed of two aluminum metasurfaces with concentric units on two sides of a thin polyimide film. Modulation is achieved by rotating the device in the normal incident wave plane. The modulation ability of the device has been verified by experimental mesurements and the finite element analysis (FEA) method based simulation. Potentially, it could be applied in THz communications and photonic computers.

2. Design and experiment

A device was designed as shown in Fig. 1a, as a whole, that the meta atom of device can be viewed as consisting two concentrically positioned aluminum units separated by polyimide layer, the top unit is hollow rings with an outer radius $r_o = 65$ μm and inner radius $r_i = 44$ μm and the bottom one is a hollow ellipse with semi-major and semi-minor axis $r_x = 65$ μm and $r_y = 44$ μm. It also can be viewed as a layer of polyimide is sandwiched by two aluminum metasurfaces with above described configuration and dimensions. Here, the r_x (r_o) and r_y (r_i) have been optimized, and detailed information can be found in the supplementary materials.

The periodicities of *meta*-atoms along both × and y directions are 150 μm. The thickness of both the top and bottom aluminum layer is 290 nm with electric conductivity of $\sigma = 3.72 \times 10^7$ S/m. The thickness of polyimide layer is 2.4 μm with a relative permittivity of$\varepsilon_{PI} = 3.5 + 0.035i$ [33]. The whole device is fabricated on a 500-μm-thick quartz

Table 1
Experimental characteristic values of the proposed filter.

f_0(THz)	T(angle = 90°)	T(angle = 0°)	w (GHz)	Q-value	MD
0.481	0.7008	0.0325	176.6	2.725	95.36%
0.931	0.0161	0.6778	260.5	3.574	97.62%

f_0: Resonant frequency, T: Transmittance, w: Full width at half maximum, MD: Modulation depth of transmission.

substrate with a refractive index $n_{quartz} = 1.96$ in the THz range. Finite element method based simulations were conducted on above device through CST Microwave Studio. There, periodic boundary conditions are set on the lateral faces of the unit to obtain an infinite metasurface. Meanwhile, the open boundary is defined to eliminate the reflection from the front face and back face. The simulation is based on Floquet's principle, where an infinite plane wave illuminates a periodic structure in the x-y plane without boundaries. Practically, scattering must be considered for a filter with a finite number of periodic units unless the dimension of the device is not comparable with the spot size of the incident wave, which is the case in our simulations.

Fig. 1b shows the simulated switching modulations to the incident wave with the variation of the polarization. The angle between the E-field and the semi-major axis r_x is defined as the rotation angle, and the direction of the semi-major axis r_x is the initial position (rotation angle = 0°). According to above design, devices have been fabricated and the optical images of a device are shown in Fig. 2a and b. It should be noted that, misalignment between the two layers of the structure could potentially impact the results (see Fig. S9). To ensure precise alignment between the two layers during fabrication, careful photolithography procedure was employed. The details of device fabrication procedure can be found in the supplementary information.

Fig. 2c shows the measured spectra at different rotation angles of the device, they are initially acquired with a THz time-domain spectroscopy (THz-TDS) system [34]. The THz-TDS system utilized in this experiment possesses a resolution of 1.56 GHz in the range of 0.1 to 3 THz. The experimentally measured spectra and the simulations are almost

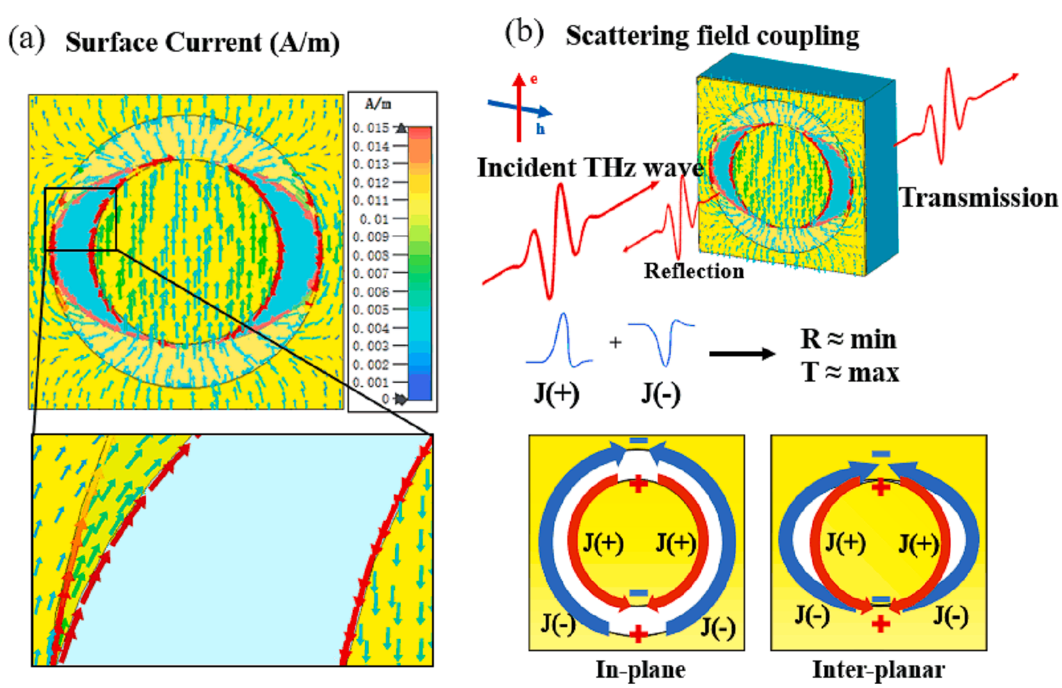

Fig. 3. (a) Surface current distribution on the metasurfaces. (b) Illustration of the "trapped mode" excitations with in-plane and inter-planar.

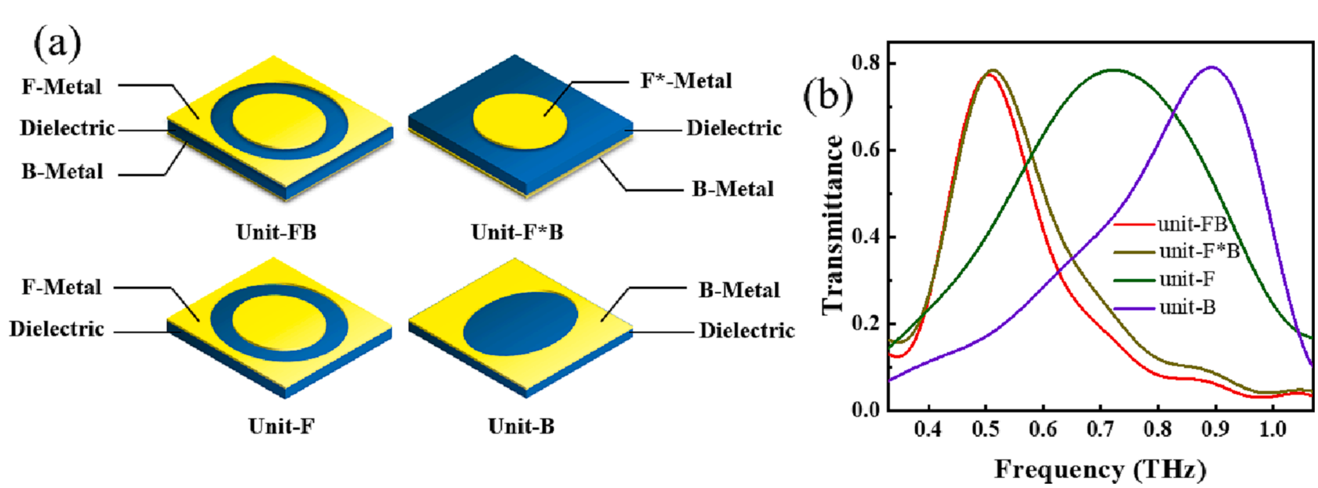

Fig. 4. (a) Structures of *unit-FB*, *unit-F*B*, *unit-F*, and *unit-B*. (b) Transmittance spectra with 90° polarized incident waves.

Table 2
The quality factor and half peak width results corresponding to the four structures at 90° polarized incidence in simulations.

	Unit-FB	Unit-F*B	Unit-F	Unit-B
Q-value	2.71	2.43	1.62	2.81
w (GHz)	186.2	211.1	446.9	318.2

w: Full width at half maximum.

identical, the minute deviations in both the characteristic frequencies and amplitude can be attributed to the device fabrication errors and unavoidable absorption of THz wave in the air.

The measured transmission curves at angles 0° and 90° are shown in Fig. 2d, and featured data are listed in Table 1. It shows that the dominant resonance frequency changes from 0.931 THz to 0.481 THz with the rotation of incident wave polarization from 0° to 90°. When the polarization oriention is in between those two limits, both two resonances co-exist but with lower transmittance as shown in Fig. 2c. The high signal-to-noise can be attributed to the large difference of two resonance frequencies that is 0.45 THz almost twice the bandwidth, hence, leading to the weak interferences between them.

3. Discussion

Surface current distribution of the device with 90° rotating polarization is simulated and analyzed as one of the particular responses. As shown in Fig. 3a, the induced currents flow in opposite directions along the edges of the outer and inner parts of the *meta*-atom. The “trapped mode” response usually exists in metamaterials consisting of subwavelength particles with structural asymmetry [35,36]. Particularly, there are two types of “trapped mode” response in this device: in-plane and inter-planar, which represents the combined pattern of two opposing currents as illustrated in Fig. 3b.

The two coexisted modes of “trapped mode” diminish the induced dipole moment, hence, weaken their coupling to the incident wave. The scattered field from the induced opposite-direction surface currents yield two coherent scattering waves with opposite phases that lead to their destructive superposition, which causes the incident wave to pass through the structure with high transmission in a narrow frequency range. Although the in-plane “trapped mode” has already been used to explain high-quality resonant response in many 2D structures [37,38], the combination of two anti-phase “trapped mode” excitation here, in our proposed metasurfaces, is novel.

In order to systematically explore the effects of these two “trapped mode” in our devices, three other related structures are introduced, named *unit-F*B*, *unit-F*, and *unit-B*, and the proposed structure is *unit-FB* for comparison, as shown in Fig. 4a, where F and B standing for the ‘Front’ and ‘back’. The *unit-F,* and *unit-B* represent the structure only have the front or back metasurfaces in the proposed structure. The *unit-F*B* is similar to the proposed structure but the front metasurface with the inner round shape structure only. The simulated transmittance spectra of these structures are shown in Fig. 4b, the Q-value and bandwidth are listed in Table 2 for comparison.

Compared with the single metal layer *meta*-atom structures, the performance of the double metal layer sandwiched *meta*-atom structures, including *unit-FB,* and *unit-F*B*, shows higher Q-value and narrower bandwidth. Particularly for *unit-FB,* it has even narrower half-peak width and larger Q-value than the *unit-F*B* and similar transmittance. Same conclusion is also held for 0° polarization (as shown in Fig. S5). These relate to the trapped mode resonance, the surface current distributions of these structures at response frequencies can be found in Fig. S6. The single *unit-B* only has symmetrical edge current distribution, therefore, does not produce “trapped mode” resonance, which lead to the broad bandwidth. Additionally, the surface current distributions of *unit-F* show the presence of the in-plane “trapped mode” coupling effect but extremely weak, *unit-F*B* demonstrates intense inter-planar “trapped mode” coupling effect which makes a sharp transmission window. These results indicate that the stronger coupling is the key factor to gain a higher Q-factor for the devices. Compared to the conventional in-plane “trapped mode”, the addition of inter-planar resonance offers an effective approach to realize an extremely narrow bandpass.

The simulated transmittance properties of this bandpass filter can be understood as a result of the combination of two resonance modes, “Mode A” and “Mode B”, and the two modes corresponds to the relative polarization orientation of impinge wave at 0° and 90° with the X-axis, respectively, as shown in Fig. 5a. Their surface current distributions can be found in Figs. S7 and S8. The two modes yield two transparent windows at two different frequencies. When the polarization of impinging wave is parallel to the X direction, mode A is strongly excited to form the transparent window in the right side; When the polarization of impinging wave is along Y direction, mode B will be ignited resulting in the formation of transparent window in the left side; When the polarization is in between, then the relative transimittance or amplitude of two windows monotonically change with the variation of the relative angle of polarization orientation of impinge wave with X-axis (or Y-axis) as shown in Fig. 5b, hence, the continuous tuning of transmistance of the waves at the resonance frequencies wave can be realized by simply rotating the device.

4. Conclusion

In this work, we propose a dual-frequency switchable narrow

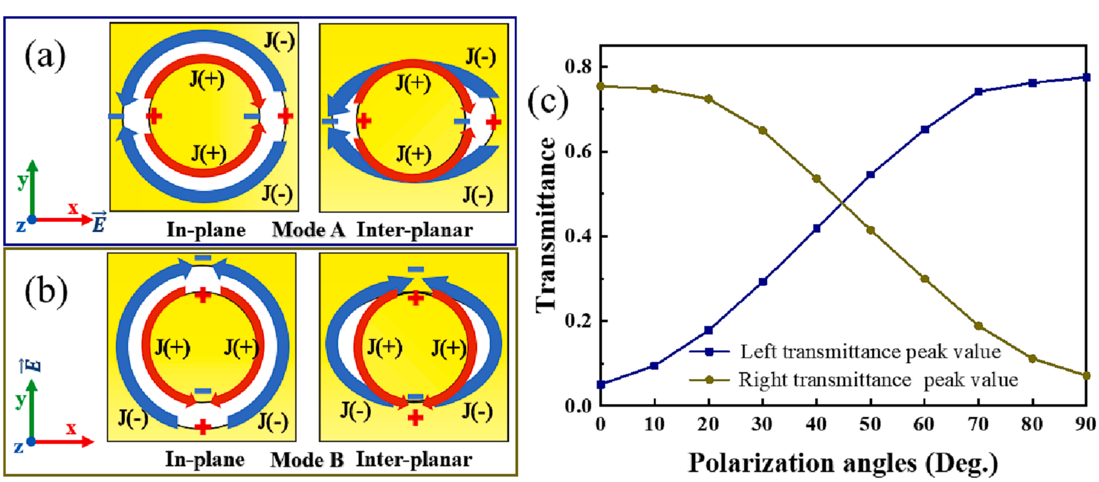

Fig. 5. The illustration of resonance (a) “Mode A” and (b) “Mode B”. (c) Transmittance at the resonance frequency for polarization angle from 0° to 90°.

bandpass filter for polarized THz waves. For the two perpendicular polarization orientation at 0° and 90°, it reaches modulation depths of 97.62 % and 95.36% with bandwidths of 260.5 GHz and 176.6 GHz and transmittances of 67.78% and 70.08% at the two resonance frequencies of 0.481 THz and 0.931 THz, respectively. Through simple rotation of the bandpass filter in the plane vertical to the incident wave, the transmittance spectrum can be switched from one resonant frequency to another. Numerical analysis unveiled that the weak coupling of the incident wave with the induced asymmetric antiphase surface currents results in the high transmittance at the resonance frequencies. This simple designed tunable bandpass filter potentially can be utilized for THz modulators and other applications.

CRediT authorship contribution statement

Yi Zhang: Methodology, Investigation, Data curation, Writing – original draft. **Dongxun Yang:** Methodology, Investigation, Data curation, Writing – original draft. **Dan Zhao:** . **Danni Hao:** Methodology, Investigation. **Pinggen Zou:** . **Yanmei Ren:** . **Rui Li:** . **Xiaodong Zhu:** . **Fei Fan:** . **Shengjiang Chang:** . **Ramiro Moro:** Writing – review & editing. **Lei Ma:** Conceptualization, Supervision, Methodology, Validation, Writing – review & editing, Funding acquisition, Project administration.

Declaration of Competing Interest

The authors declare that they have no known competing financial interests or personal relationships that could have appeared to influence the work reported in this paper.

Data availability

Data will be made available on request.

Acknowledgments

This work was supported by the National Natural Science Foundation of China (11774255) and the National Key R&D Program of China (2020YFC2004602).

Appendix A. Supplementary data

Supplementary data to this article can be found online at https://doi.org/10.1016/j.cplett.2023.140637.

References

[1] M. Nagel, M. Först, H. Kurz, THz biosensing devices: fundamentals and technology, J. Phys. Condens. Matter 18 (2006) S601–S618.
[2] J. Zhou, X. Zhao, G. Huang, X. Yang, Y. Zhang, X. Zhan, H. Tian, Y. Xiong, Y. Wang, W. Fu, Molecule-specific terahertz biosensors based on an aptamer hydrogel-functionalized metamaterial for sensitive assays in aqueous environments, ACS Sens. 6 (2021) 1884–1890.
[3] P.U. Jepsen, D.G. Cooke, M. Koch, Terahertz spectroscopy and imaging - Modern techniques and applications, Laser Photon. Rev. 5 (2011) 124–166.
[4] K.B. Cooper, G. Chattopadhyay, Submillimeter-wave radar: solid-state system design and applications, IEEE Microw. Mag. 15 (2014) 51–67.
[5] L. Wei, L. Yu, H. Jiaoqi, H. Guorong, Z. Yang, F. Weiling, Application of terahertz spectroscopy in biomolecule detection, Front. Lab. Med. 2 (2018) 127–133.
[6] H.-J. Song, T. Nagatsuma, Present and future of terahertz communications, IEEE Trans. Terahertz Sci. Technol. 1 (2011) 256–263.
[7] R.A. Lewis, A review of terahertz sources, J. Phys. D Appl. Phys. 47 (37) (2014) 374001.
[8] Z.T. Ma, Z.X. Geng, Z.Y. Fan, J. Liu, H.D. Chen, Modulators for Terahertz communication: the current state of the art, Research 2019 (2019) 6482975.
[9] R.A. Lewis, A review of terahertz detectors, J. Phys. D Appl. Phys. 52 (43) (2019) 433001.
[10] J. Shi, Z. Li, D.K. Sang, Y. Xiang, J. Li, S. Zhang, H. Zhang, THz photonics in two dimensional materials and metamaterials: properties, devices and prospects, J. Mater. Chem. C 6 (2018) 1291–1306.
[11] M. Manjappa, P. Pitchappa, N. Singh, N. Wang, N.I. Zheludev, C. Lee, R. Singh, Reconfigurable MEMS Fano metasurfaces with multiple-input-output states for logic operations at terahertz frequencies, Nat. Commun. 9 (2018) 4056.
[12] R. Xu, X. Xu, B.-R. Yang, X. Gui, Z. Qin, and Y.-S. Lin, "Actively logical modulation of MEMS-based terahertz metamaterial," Photon. Res. **9**, 1409 (2021).
[13] S. Moghaddas, M. Ghasemi, P.K. Choudhury, B.Y. Majlis, Engineered metasurface of gold funnels for terahertz wave filtering, Plasmonics 13 (2017) 1595–1601.
[14] C.-C. Chang, L. Huang, J. Nogan, H.-T. Chen, Invited Article: Narrowband terahertz bandpass filters employing stacked bilayer metasurface antireflection structures, APL Photon. 3 (2018), 051602.
[15] M.T. Nouman, H.W. Kim, J.M. Woo, J.H. Hwang, D. Kim, J.H. Jang, Terahertz Modulator based on Metamaterials integrated with Metal-Semiconductor-Metal Varactors, Sci. Rep. 6 (2016) 26452.
[16] E. Kaya, N. Kakenov, H. Altan, C. Kocabas, O. Esenturk, Multilayer graphene broadband terahertz modulators with flexible substrate, J. Infrared Millimeter Terahertz Waves 39 (5) (2018) 483–491.
[17] Q. Li, Z. Tian, X. Zhang, R. Singh, L. Du, J. Gu, J. Han, W. Zhang, Active graphene-silicon hybrid diode for terahertz waves, Nat. Commun. 6 (2015) 7082.
[18] Y. Wen, W. Ma, J. Bailey, G. Matmon, G. Aeppli, X. Yu, Absorption modulation of terahertz metamaterial by varying the conductivity of ground plane, Appl. Phys. Lett. 105 (14) (2014) 141111.
[19] M. Huang, Y. Cheng, Z. Cheng, H. Chen, X. Mao, R. Gong, Based on graphene tunable dual-band terahertz metamaterial absorber with wide-angle, Opt. Commun. 415 (2018) 194–201.
[20] F. Yan, Q. Li, Z. Wang, H. Tian, L. Li, Extremely high Q-factor terahertz metasurface using reconstructive coherent mode resonance, Opt. Express 29 (2021) 7015–7023.
[21] A. Ahmadivand, B. Gerislioglu, Z. Ramezani, Gated graphene island-enabled tunable charge transfer plasmon terahertz metamodulator, Nanoscale 11 (2019) 8091–8095.
[22] M.S. Islam, J. Sultana, M. Biabanifard, Z. Vafapour, M.J. Nine, A. Dinovitser, C.M. B. Cordeiro, B.W.H. Ng, D. Abbott, Tunable localized surface plasmon graphene metasurface for multiband superabsorption and terahertz sensing, Carbon 158 (2020) 559–567.
[23] Y. Sun, D. Liao, J. Xu, Y. Wu, L. Chen, Active Switching of Toroidal Resonances by Using a Dirac Semimetal for Terahertz Communication, Front. Phys. 8 (2020).
[24] J.-H. Shin, K.H. Park, H.-C. Ryu, Electrically controllable terahertz square-loop metamaterial based on VO(2) thin film, Nanotechnology 27 (19) (2016) 195202.
[25] N. Born, A. Crunteanu, G. Humbert, A. Bessaudou, M. Koch, B.M. Fischer, Switchable THz Filter Based on a Vanadium Dioxide Layer Inside a Fabry-Pérot Cavity, IEEE Trans. Terahertz Sci. Technol. 5 (2015) 1035–1039.
[26] X. Fan, Y. Li, S. Chen, Y. Xing, T. Pan, Mechanical Terahertz Modulation by Skin-Like Ultrathin Stretchable Metasurface, Small 16 (37) (2020) 2002484.
[27] F. Lu, H. Ou, Y.S. Lin, Reconfigurable terahertz switch using flexible L-shaped metamaterial, Opt. Lett. 45 (2020) 6482–6485.
[28] M. Kafesaki, N.H. Shen, S. Tzortzakis, C.M. Soukoulis, Optically switchable and tunable terahertz metamaterials through photoconductivity, J. Opt. 14 (11) (2012) 114008.
[29] W.B. He, M.Y. Tong, Z.J. Xu, Y.Z. Hu, X.A. Cheng, T. Jiang, Ultrafast all-optical terahertz modulation based on an inverse-designed metasurface, Photon. Res. 9 (2021) 1099–1108.
[30] R. Ortuño, C. García-Meca, A. Martínez, Terahertz metamaterials on flexible polypropylene substrate, Plasmonics 9 (2014) 1143–1147.
[31] A. Ahmadivand, B. Gerislioglu, N. Pala, Large-modulation-depth polarization-sensitive plasmonic toroidal terahertz metamaterial, IEEE Photon. Technol. Lett. 29 (2017) 1860–1863.
[32] X. Xu, R. Xu, Y.-S. Lin, Tunable terahertz double split-ring metamaterial with polarization-sensitive characteristic, Opt. Laser Technol. 141 (2021) 107103.
[33] XiaoFei Zang, HanHong Gong, Z. Li, JingYa Xie, QingQing Cheng, L. Chen, A. P. Shkurinov, YiMing Zhu, SongLin Zhuang, Metasurface for multi-channel terahertz beam splitters and polarization rotators, Appl. Phys. Lett. 112 (17) (2018) 171111.
[34] L. Chen, D.-G. Liao, X.-G. Guo, J.-Y. Zhao, Y.-M. Zhu, S.-L. Zhuang, Terahertz time-domain spectroscopy and micro-cavity components for probing samples: a review, Front. Inform. Technol. Electron. Eng. 20 (2019) 591–607.
[35] V.R. Tuz, V.V. Khardikov, A.S. Kupriianov, K.L. Domina, S. Xu, H. Wang, H.B. Sun, High-quality trapped modes in all-dielectric metamaterials, Opt. Express 26 (2018) 2905–2916.
[36] S. Yang, Z. Liu, X. Xia, Y. E, C. Tang, Y. Wang, J. Li, L.i. Wang, C. Gu, Excitation of ultrasharp trapped-mode resonances in mirror-symmetric metamaterials, Phys. Rev. B 93 (23) (2016), 235407.
[37] V. Khardikov, E. Iarko, and S. Prosvirnin, "Trapped mode resonances in optical planar periodical structures with metal and dielectric elements," presented at the 2010 International Conference on Mathematical Methods in Electromagnetic Theory2010.
[38] S. Prosvirnin, N. Papasimakis, V. Fedotov, S. Zouhdi, N. Zheludev, Trapped-Mode Resonances in Planar Metamaterials with High Structural Symmetry, in: S. Zouhdi, A. Sihvola, A.P. Vinogradov (Eds.), NATO Science for Peace and Security Series B: Physics and BioPhysicsMetamaterials and Plasmonics: Fundamentals, Modelling, Applications, Springer Netherlands, Dordrecht, 2009, pp. 201–208.